Available online at www.sciencedirect.com
SCIENCE DIRECT®
ELSEVIER
Journal of Magnetism and Magnetic Materials 279 (2004) 202–209
Journal of magnetism and magnetic materials
www.elsevier.com/locate/jmmm

Structural and magnetic properties of Al doped Co–Ag granular films: temperature dependence of magnetoresistance

R. Mustafa Öksüzoglu[a,*], Ayhan Elmali[b], Rüdiger Henn[c], Hartmut Fuess[d], Horst Hahn[d]

[a] *Faculty of Science and Art, Department of Physics, University of Selcuk, Campus, Konya 42031, Turkey*
[b] *Faculty of Engineering, Department of Engineering Physics, Ankara University, Besevler, Ankara 06100, Turkey*
[c] *Max-Planck-Institut für Festkörperforschung, Heisenbergstr. 1, Stuttgart D-70569, Germany*
[d] *Institute for Materials Science, Darmstadt University of Technology, Petersenstrasse 23, Darmstadt D-64287, Germany*

Received 28 August 2003; received in revised form 21 January 2004

Abstract

The correlation between the structure, the magnetic and magnetotransport properties of sputter-deposited $(Co_{90}Al_{10})_xAg_{100-x}$ granular films ($19 \leqslant x \leqslant 45$) are investigated. For an $(Co_{90}Al_{10})$ content of about 28% the magnetoresistance (MR) ratio of the films reach its highest value of 6%. Al doping reduces the MR ratio in CoAg films, however, leads to a almost constant MR ratio against post annealing up to 773 K in $(Co_{90}Al_{10})_{28}Ag_{72}$ granular films, although the film structure is affected by annealing, respectively. According to magnetization measurements, superparamagnetic cobalt grains in the as-deposited $(Co_{90}Al_{10})_{28}Ag_{72}$ sample show after annealing up to 773 K both superparamagnetic and ferromagnetic behaviour. Annealing at 823 K causes a domain formation of large ferromagnetic grains with strong correlation.

PACS: 75.47.De; 75.70.Cn; 68.55.Jk; 81.15.Cd

Keywords: Magnetoresistance; Magnetic properties of heterostructures; Structural properties; Sputtering

1. Introduction

The giant magnetoresistance (GMR) effect in magnetic multilayers and subsequently in magnetic heterogeneous alloys with ferromagnetic granules embedded in nonmagnetic metals has been intensively studied over the last 10 years [1–8]. In particular, the CoAg granular films, exhibiting the largest GMR value at room temperature, were extensively investigated [1,4,8,9–12]. In granular systems, the GMR effect is caused by spin-dependent scattering at the interfaces between the ferromagnetic grains and the nonmagnetic matrix and spin-dependent scattering within ferromagnetic grains [13,14]. In addition, the GMR effect is influenced by the size of ferromagnetic grains [8]. As annealing causes grain growth the thermal

*Corresponding author. Tel.: +0090-332-223-1844; fax: +0090-332-241-0604.
E-mail address: rmoksuzoglu@selcuk.edu.tr (R.M. Öksüzoglu).

0304-8853/$ - see front matter © 2004 Elsevier B.V. All rights reserved.
doi:10.1016/j.jmmm.2004.01.080

treatment is of considerable importance. Annealing causes increment of the grain size in the granular films. Previous studies show that the GMR value is affected both by deposition [9], and post-annealing temperature [1,8]. Furthermore, the annealing dependent fine differences in the microstructure – defect healing and/or changes in interfacial structure – have also considerable impact on the GMR behaviour of the CoAg granular films [11]. To reduce the saturation field in coupled systems some methods were used which influenced the interlayer coupling between ferromagnetic layers. The studies on GMR multilayer structures showed that the saturation/switching field can be reduced by addition of a small amount of Al in Co layer [15], or Mn in Cu spacer [16], in Co/Cu multilayer structures. One might easily ask what the situation would be if the magnetic metal is doped with Al or Mn in the granular films. Al was chosen as impurities in the CoAg system since Al does not form intermetallic compounds with Co and Ag. The intermetallic compounds only take place after annealing. The aim of the present study was to investigate the influence of a small amount of Al on the saturation field of magneto resistance, on magnetic properties and on the structure of CoAg granular films, as well as the dependence of the post-annealing temperature. We then correlate the structural properties with the resultant magnetic and magneto transport characteristics.

2. Experimental procedures

The samples investigated were prepared at room temperature by DC magnetron sputtering onto Si substrates with a 1000 nm SiO_2-buffer layer. The target materials were 99.9% purity $Co_{90}Al_{10}$ and Ag (K.J. Lesker Company, UK). The argon pressure during the preparation of the films was adjusted at 7.5 m Torr by a gas-flow controller. The base pressure was better than 1×10^{-7} Torr. The sample thickness and the composition of the films were determined by calibrated quartz crystal monitors. The deposition rates were between 1.0 and 3.4 Å/s for Ag and maintained for $(Co_{90}Al_{10})$ at 0.8 Å/s, respectively (nominal composition $(Co_{90}Al_{10})_xAg_{100-x}$, $x = 19-45$, respectively). The thickness of all samples amount to about 200 nm determinated by the sputtering time and rate. Furthermore, the structure of the film was investigated by grazing incidence X-ray diffraction (GIXD). A Bragg–Soller X-ray diffractometer system with a flat secondary monochromator and fixed CuK_α tube (Seifert XRD 3000 TT) was used at low incidence ($\Omega = 1^\circ$) with 2Θ scan. Zero field- and field cooling (ZFC, FC) and magnetization measurements were carried out by a SQUID magnetometer (maximum applied field 6 T) in the temperature range of 5–300 K. The magnetoresistance (MR) ratio – $\Delta R/R = [R(0) - R(1.5\,T)]/R(0)$ – was measured by a standard four terminal DC technique with the magnetic field perpendicular to the sample current. Both the magnetic field and sample current were adjusted parallel to the film plane. Post-deposition thermal annealing of the samples was carried out under high vacuum (better than 1×10^{-6} Torr) at temperatures between 373 and 773 K for 15 min (short-term annealing, STA) and at 823 K for 30 min (long-term annealing, LTA) with ramp rate of 10°C/min and natural cooling. The GIXD, magnetic and electrical measurements were performed after each annealing process to achieve best correspondence among these measurements.

3. Results and discussion

3.1. Structural properties

GIXD patterns of the as-deposited samples, with different $(Co_{90}Al_{10})$ volume fraction, indicate a highly $\langle 1\,1\,1 \rangle$ textured structure of FCC silver (Fig. 1a), but no firm crystallographic evidence of either fcc or hcp cobalt in the as-deposited state. The intensity of Ag(1 1 1) peak decreases with increasing $(Co_{90}Al_{10})$ volume fraction. The diffraction angles were corrected by grazing incidence angle. Compared to pure Ag, the diffraction angles for Ag(1 1 1) are almost unchanged till $x = 23\%$ and are successively shifted to higher angles for $x > 23\%$. Consequently, the lattice spacing for Ag(1 1 1) – $d_{Ag(1\,1\,1)}$ – decreases with increasing $(Co_{90}Al_{10})$ volume fraction (see Fig. 1b). This effect, i.e. the contraction of the Ag lattice must be

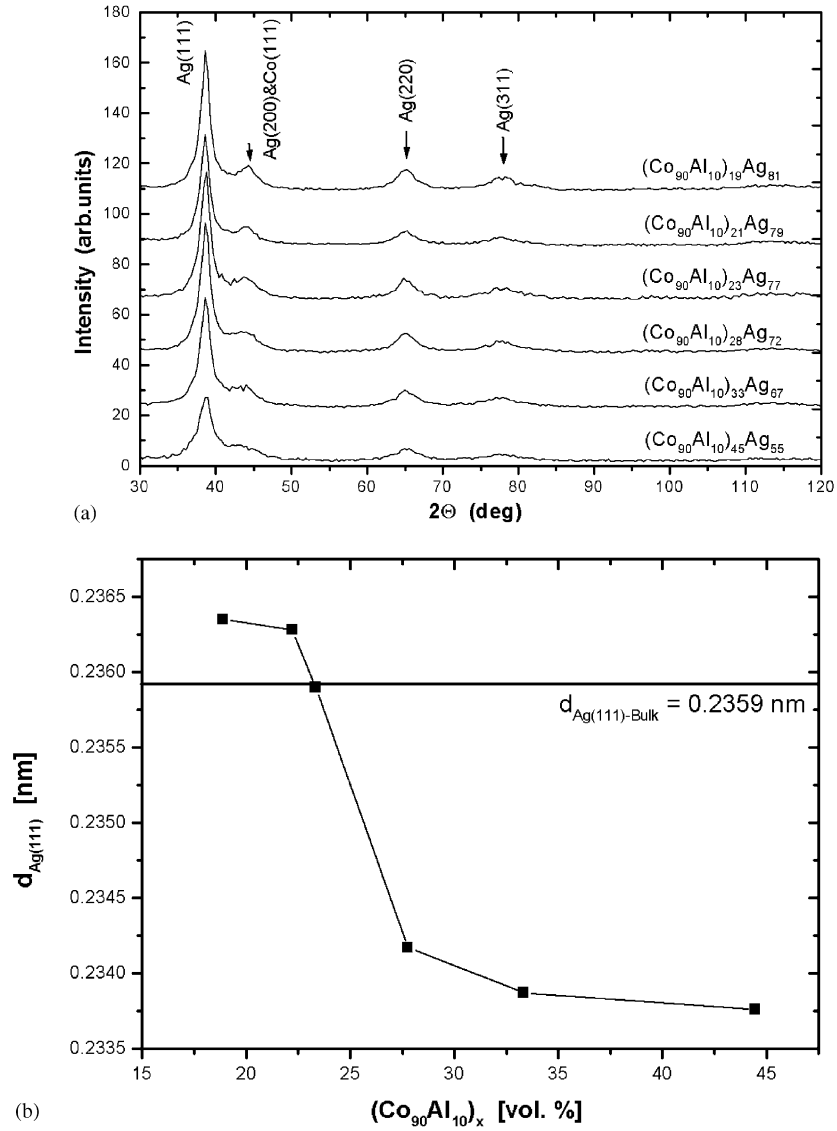

Fig. 1. (a) GIXD pattern for as-deposited $(Co_{90}Al_{10})_xAg_{100-x}$ samples ($T_S = 300\,K$) as a function of $(Co_{90}Al_{10})$ content ($x = 19-45$ vol%). All patterns are indexed by Ag (1 1 1), Ag (2 0 0), Ag (2 2 0) and Ag (3 1 1) diffraction lines. (b) Evolution of lattice spacing for Ag (1 1 1) reflection as a function of $(Co_{90}Al_{10})$ content.

associated with the partial substitution of Ag atoms by the smaller Co or Al atoms at higher volume fractions. In our previous investigation, the analysis of SAED patterns of the as-deposited sample confirmed the presence of FCC Ag as dominant phase whilst reflections from cobalt are apparently absent [17].

The effect of the post-thermal treatment on the structure was investigated for the $(Co_{90}Al_{10})_{28}Ag_{72}$ sample with highest MR value. After each annealing step the MR, GIXD measurements and investigations using electron spectroscopic images (ESI) were carried out, in order to establish a correlation between structure and magneto

transport properties. The distribution of cobalt clusters in the films obtained by ESI maps has already been reported [17]. The GIXD patterns for different post-annealing temperatures are shown in Fig. 2a. In comparison to the as-deposited sample, a second set of weak intensity fcc diffraction peaks emerges after annealing at 673 K, indicating the formation of small fcc Co particles in an fcc Ag-matrix. The intensity of the Ag(1 1 1) peak reveals again the high $\langle 1\,1\,1 \rangle$ textured structure of silver. The intensity of that peak increases with increasing annealing temperature and the lattice spacing for Ag(1 1 1) – $d_{\mathrm{Ag(1\,1\,1)}}$ – approaches to the bulk value of pure silver at higher temperatures (Fig. 2b). Thus, the increasing temperature reduces the mismatch stress between substrate and film and of disorder and defects.

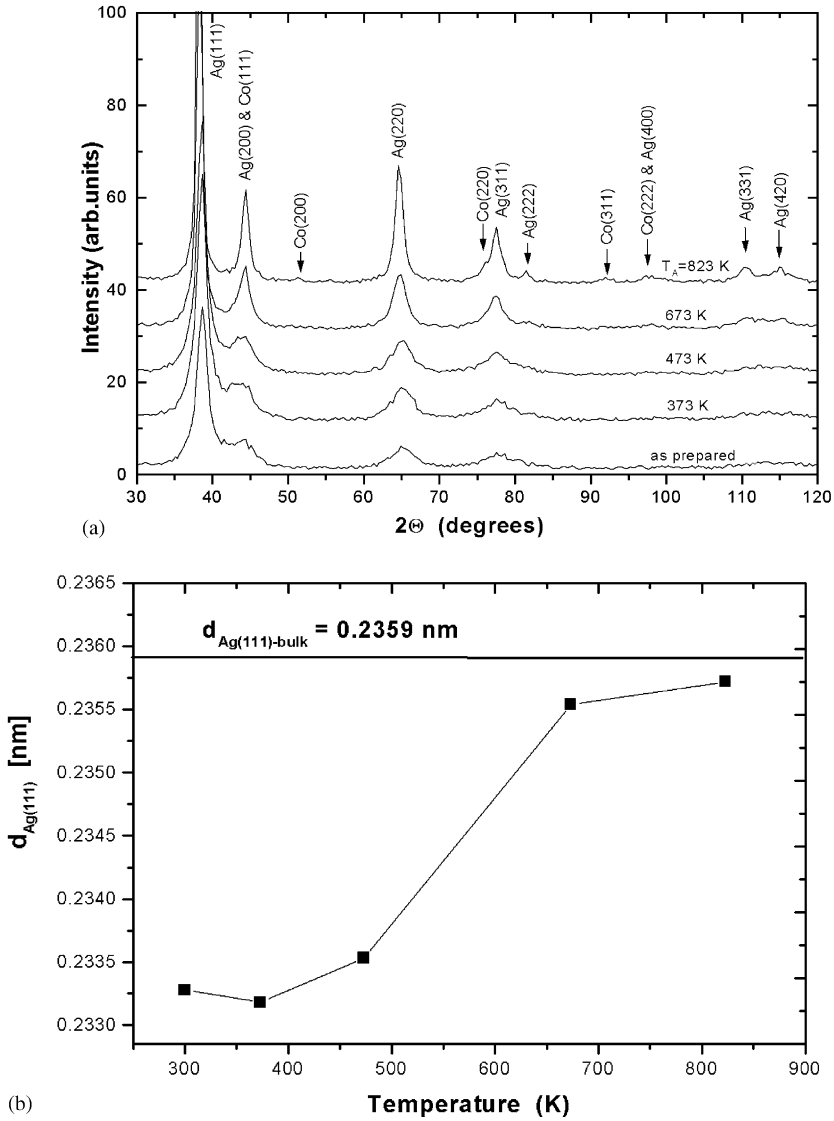

Fig. 2. (a) GIXD pattern of as-deposited and post annealed $(Co_{90}Al_{10})_{28}Ag_{72}$ samples for temperatures between 373 and 823 K. (b) Evolution of the lattice spacing for Ag (1 1 1) reflection as a function of annealing temperature in $(Co_{90}Al_{10})_{28}Ag_{72}$ sample.

The previous investigations using SAED on thermally treated $(Co_{90}Al_{10})_{28}Ag_{72}$ samples lead to additional information about the microstructure [17]. Whereas X-ray diffraction (Fig. 2a) only indicated the formation of fcc cobalt at 673 and 773 K, the results of SAED gave clear evidence of the presence of large cobalt particles of fcc and hcp structure in addition to the fcc silver matrix [17]. No additional crystalline phases from Co–Al or Ag–Al were observed as expected from the phase diagram for Co–Al and Ag–Al [L.Börn91]. However, after annealing at 823 K, the presence of small amounts of BCC Ag_3Al was detected [17].

3.2. Magnetoresistance

The composition dependence of the MR values in the $(Co_{90}Al_{10})_xAg_{100-x}$, $x = 19-45\%$) films studied is shown in Fig. 3. The MR values increase with the ferromagnetic metal content up to the optimum MR composition and then they sharply drop off at higher $(Co_{90}Al_{10})$ volume fractions. The highest value was observed for a $(Co_{90}Al_{10})_{28}Ag_{72}$ sample (28% $(Co_{90}Al_{10})$) with respective MR change of 6%. In comparison with the previously investigated $Co_{25}Ag_{75}$ films [12], showing a MR of 14%, the small amount of aluminium lead on average to a reduction of MR in CoAg system. In comparison to CoAl/Cu multilayers [15], a reduction of saturation field was not obtained.

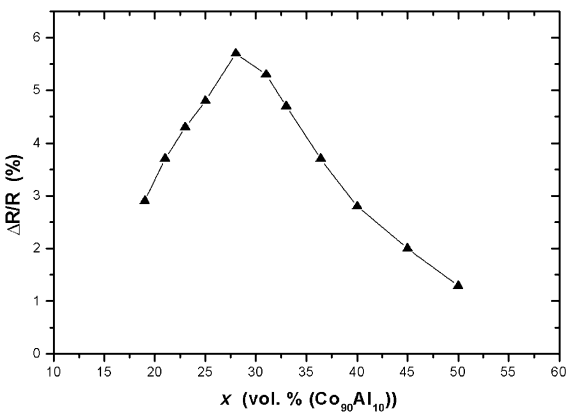

Fig. 3. The composition dependence of the GMR values in the $(Co_{90}Al_{10})_xAg_{100-x}$, $x = 19-50$ vol. %) films.

The influence of post thermal treatment on MR was investigated for $(Co_{90}Al_{10})_{28}Ag_{72}$ sample with highest MR. Three important parameters, $R(0)$, $\Delta R = R(0) - R$ (1.5 T) and $\Delta R/R(0)$ or MR ratio as a function of annealing temperature were extracted from the MR measurements as shown in Fig. 4a and b. The magnitude of MR remains almost unchanged up to 773 K for STA, but LTA at 823 K results in a decrease of MR to 3.3% (Fig. 4a). $R(0)$ and ΔR decreases almost similar with increasing temperature till 773 K (Fig. 4b), resulting in nearly constant $\Delta R/R(0)$ ratios. The ΔR indicated a slightly higher drop at 823 K (Fig. 4b), in agreement with a higher decrease in $\Delta R/R(0)$ (Fig. 4a). In agreement with previous studies, the temperature dependence of CoAg granular films was confirmed [1,9,11]. The

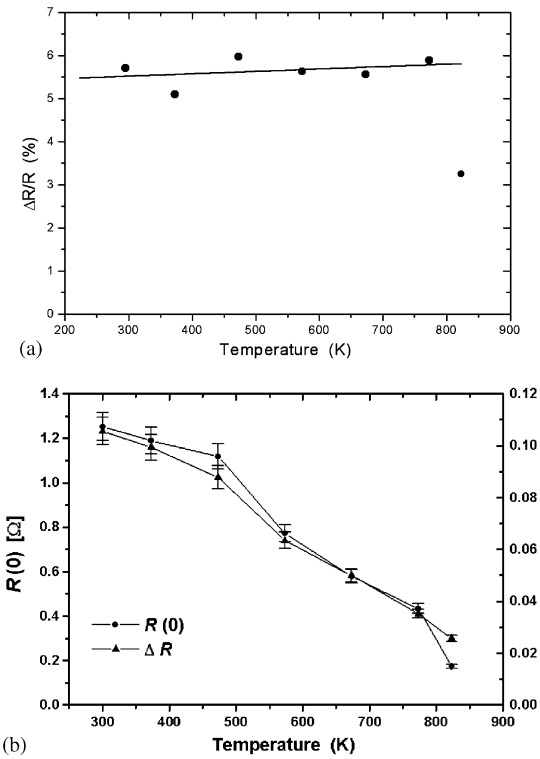

Fig. 4. (a) MR effect for the $(Co_{90}Al_{10})_{28}Ag_{72}$ samples, as-deposited and after post-annealing between 373 and 823 K. (b) Variation of the film resistance, $R(H = 0)$ (●) and ΔR (▲) with post-annealing temperature for the $(Co_{90}Al_{10})_{28}Ag_{72}$ samples.

post-annealing causes first an increase in MR and then a decrease for both STA (10 min) [1], and LTA (30 min) [11]. A similar behaviour was reported for films deposited at substrate temperatures between 300 and 723 K for CoAg [10], and between 300 and 773 K for FeAg films [8]. These authors reported that $R(0)$ decreases more rapidly than ΔR with annealing temperature causing a temperature dependence of MR as mentioned. Thermal annealing reduces the structural disorder, enlarges particle size and increases interparticle separation, leading to an increase of the electron mean free path and consequently $R(0)$ decreases. The reduction of ΔR is mainly due to the reduction of spin-dependent scattering as a result of enlarged particle size [8,18]. We assume that the small amount of aluminium embedded in the silver matrix or at cobalt particle surfaces can inhibit the enlargement of magnetic grains and the rapid reduction of the resistance. The decrease of the MR value to 3.3% after LTA at 823 K, is attributable to larger cobalt grains and to the bcc Ag_3Al phase [17], reducing the resistance more rapidly at this temperature, consequently the MR ratio.

3.3. Magnetic characterization

The thermal dependence of magnetization can provide deeper information about the actual structure of the films. Fig. 5 shows the temperature dependence of magnetization for the $(Co_{90}Al_{10})_{28}Ag_{72}$ sample as-deposited in both FC and ZFC states. The magnetization was measured at magnetic fields of 20, 200 and 300 mT. For each case, the sample was first cooled down to 5 K in zero field. The magnetization was then measured for increasing temperature (ZFC), and consecutively for decreasing temperature in an identical magnetic field (FC). For each field, the magnetization versus temperature behaviour has the following characteristic: (1) the blocking temperature (T_B) in the ZFC magnetization as the temperature increased, (2) reversible behaviour for the FC magnetization above the T_B temperature, and (3) irreversible behaviour for the FC magnetization below T_B. The features above are characteristics of superparamagnetic behaviour of magnetic grains

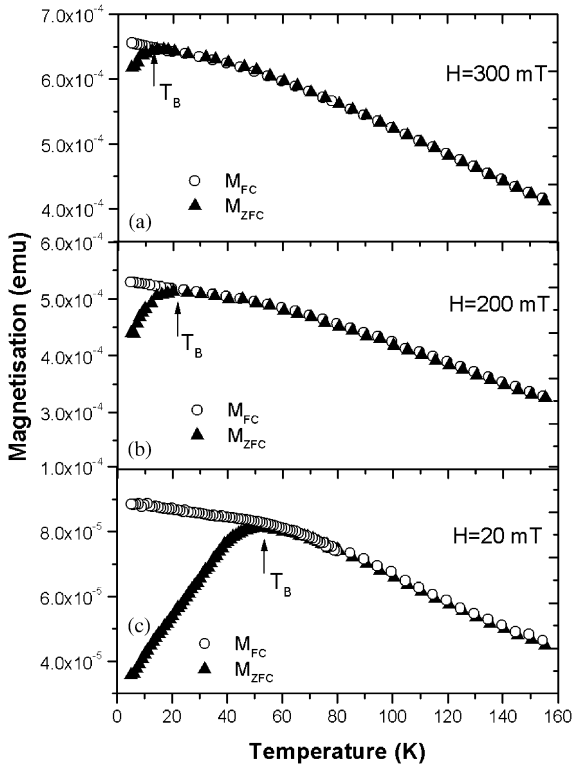

Fig. 5. Magnetic moment (arb. units) versus temperature (K) with various applied magnetic fields for the as-prepared $(Co_{90}Al_{10})_{28}Ag_{72}$ sample; open circles represent decreasing temperature of FC magnetization and solid triangles represent increasing temperature of ZFC magnetization: (a) $H = 300$ mT; (b) $H = 200$ mT; (c) $H = 20$ mT.

in granular films. The T_B increases with decreasing magnetic field (Fig. 5), and occurs at 14, 24 and 55 K for 300, 200 and 20 mT. A similar dependence of superparamagnetic blocking temperature was reported by Zhang et al. [19]. Upon post-annealing the T_B shifts to higher temperatures for applied magnetic fields (Fig. 6). The higher blocking temperature reflects the particle growth during annealing. As shown in Fig. 6, T_B remains almost unchanged for the sample annealed at 773 K, which is attributable to ferromagnetic state of the magnetic cobalt grains.

The size of ferromagnetic grains in a granular system can be indirectly estimated from the temperature dependence of magnetization (M) [19]. The M versus T behaviour was measured for the as-prepared and post-annealed $(Co_{90}Al_{10})_{28}Ag_{72}$

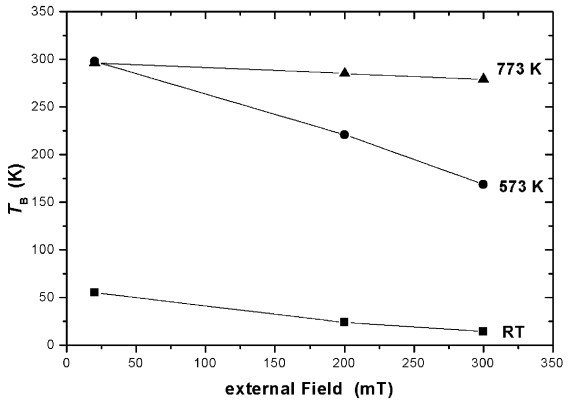

Fig. 6. The external magnetic field dependence of blocking temperature T_B for the as-deposited, and annealed $(Co_{90}Al_{10})_{28}Ag_{72}$ samples.

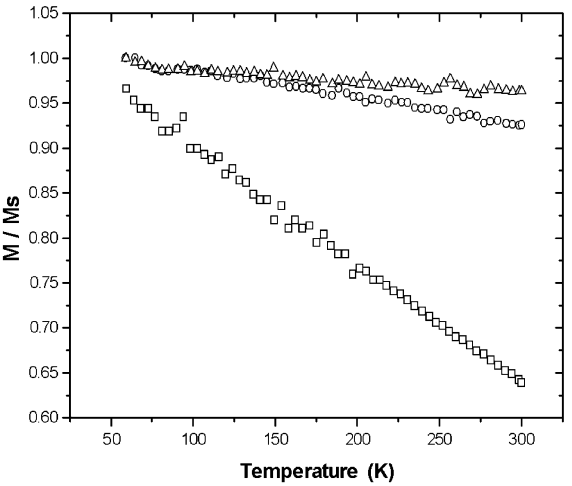

Fig. 7. The temperature dependence of magnetization (normalized to saturation magnetization) for $(Co_{90}Al_{10})_{28}Ag_{72}$ sample; as-deposited (□), annealed at 573 K (○) and 773 K (△).

samples in a magnetic field of 6 T. A linear decrease of the magnetization with increasing temperature (Fig. 7) was observed for the samples as-deposited, annealed at 573 and 773 K. These are consistent with the high-field/low-temperature approximation of the Langevin-function $M/M_s \approx 1-(k_BT/N\mu H)$ [19]. Hereby, N is the number of the cobalt atoms in the particle and μ is the magnetic moment of a single cobalt atom in a particle or grain. From the slopes of the M versus T curves (Fig. 7), and by taking $\mu_{eff} = 1.7\,\mu_B$ (the value for bulk Co), one obtains the average number of cobalt atoms in the particle, N. The number of cobalt clusters corresponds to a particle diameter of $d \approx 0.12$ Å for as-deposited, 1.9 Å for that annealed at 573 K and 3.9 Å for that at 773 K. The summary of the grain sizes estimated both from the M versus T curves and from ESI images (reported previously by [17]) are shown together in Fig. 8.

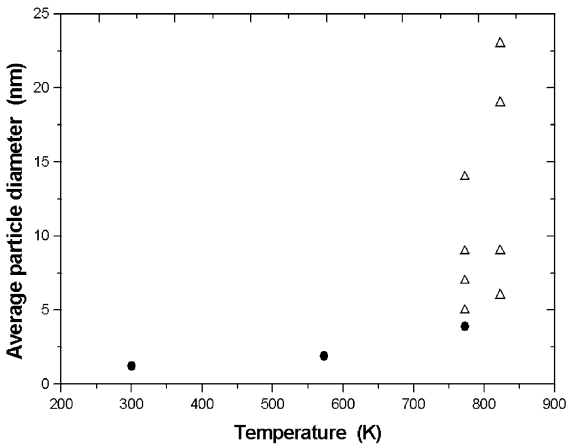

Fig. 8. The average size of cobalt particles in $(Co_{90}Al_{10})_{28}Ag_{72}$ samples for different annealing temperatures, estimated from the fitting of M versus T curves (●), and the size of cobalt clusters estimated from ESI element distribution maps (Δ) (taken from [15]).

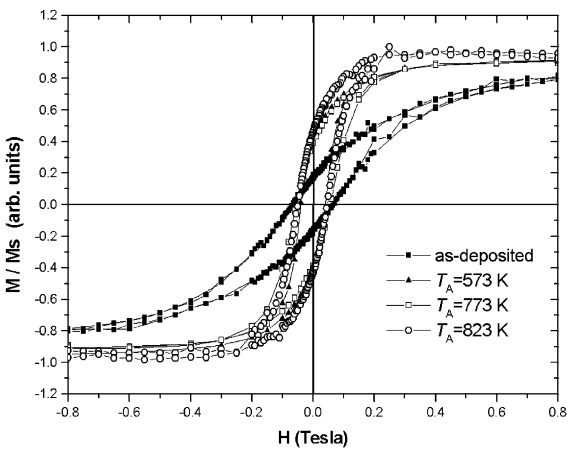

Fig. 9. Hysteresis loops of as-deposited and post-annealed $(Co_{90}Al_{10})_{28}Ag_{72}$ samples measured at 5 K.

Hysteresis curves of $(Co_{90}Al_{10})_{28}Ag_{72}$ sample as-deposited and after post-annealing are shown in Fig. 9. The saturation field and form of the $M-H$ loop can be attributed to the magnetic character of the grains in the film. The $M-H$ loop in Fig. 9 for an as-deposited sample has a characteristic form for superparamagnetic grains in the granular films. With increasing annealing temperature the $M-H$ loops saturate at lower magnetic fields and become broader, indicating the existence of larger grains with ferromagnetic behaviour. After LTA at 823 K, the saturation field is lower compared to that with STA at 573 and 773 K. This is attributable to a domain formation of large ferromagnetic grains with strong correlation. Those are in good agreement with increased blocking temperature T_B in ZFC–FC measurements after annealing and grain sizes estimated from ESI images (Fig. 8).

4. Conclusion

Compared to previous investigations, in the present study a new granular film system consisting of Co–Ag–Al, has been investigated and the correlation between structural and magnetic transport properties is discussed. Addition of small amounts of Al in CoAg granular film leads to a reduction of MR, but the MR remains almost unchanged by STA up to 773 K. In comparison to CoAg films, the increase of cobalt grain size with increasing STA temperature did not influence the MR ratio in $(Co_{90}Al_{10})_{28}Ag_{72}$ films. In comparison, the LTA at 823 K causes a pronounced structural difference by the formation of bcc Ag_3Al besides fcc Ag and larger and broader distributed cobalt grains in the sample. As a result, addition of aluminium with very slight solubility in silver leads to new temperature behaviour in granular Co–Ag films.

Acknowledgements

Financial support from the Fonds Deutschen Chemischen Industrie is gratefully acknowledged.

References

[1] J.Q. Xiao, J.S. Jiang, C.L. Chien, Phys. Rev. B 46 (1992) 9266.
[2] J.A. Barnard, A. Waknis, M. Tan, E. Haftek, M.R. Parker, M.L. Watson, J. Magn. Magn. Mater. 114 (1992) L230.
[3] A.E. Berkowitz, M.J. Carey, J.R. Mitchell, A.P. Young, S. Zhang, F.E. Spada, F.T. Parker, A. Hutten, G. Thomas, Phys. Rev. Lett. 68 (1992) 3745.
[4] A.E. Berkowitz, J.R. Mitchell, M.J. Carey, A.P. Young, D. Rao, A. Starr, S. Zhang, F.E. Spada, F.T. Parker, A. Hutten, G. Thomas, J. Appl. Phys. 73 (1993) 5320.
[5] M.J. Carey, A.P. Young, A. Starr, D. Rao, A.E. Berkowitz, Appl. Phys. Lett. 61 (1992) 2935.
[6] G. Xiao, J. Wang, P. Xiong, Appl. Phys. Lett. 62 (1993) 420.
[7] F. Conde, C. Gomez-Polo, A. Henando, J. Magn. Magn. Mater. 138 (1994) 123.
[8] J.-Q. Wang, G. Xiao, Phys. Rev. B 49 (II) (1994) 3982.
[9] A. Azizi, S.M. Thompson, K. Ounadjela, J. Gregg, P. Vennegues, A. Dinia, J. Arabski, C. Fermon, J. Magn. Magn. Mater. 148 (1995) 313.
[10] K. Ounadjela, S.M. Thompson, J.F. Gregg, A. Azizi, M. Gester, J.P. Deville, Phys. Rev. B 54 (I) (1996) 12252.
[11] J.H. Du, W.J. Liu, Q. Li, H. Sang, S.Y. Zhang, Y.W. Du, D. Feng, J. Magn. Magn. Mater. 191 (1999) 17.
[12] R.M. Öksüzoglu, A. Elmali, T.E. Weirich, H. Fuess, H. Hahn, J. Phy.: Condens. Matter 12 (2000) 9237.
[13] P.M. Levi, J. Magn. Magn. Mater. 140–144 (1995) 485.
[14] S. Zhang, P.M. Levy, J. Appl. Phys. 73 (1993) 5315.
[15] S.M. Zhou, L.Y. Chen, W.M. Zheng, W.R. Zhu, Y. Wang, Y.D. Wang, Y.X. Zheng, Q.Y. Jin, Y.H. Qian, Appl. Phys. Lett. 69 (1996) 127.
[16] H. Wang, Q.Y. Jin, S.M. Zhou, Y.H. Shen, F.M. Li, L.Y. Chen, S.R. Zhu, H.L. Shen, M.H. Pan, M. Lu, J. Appl. Phys. 85 (1999) 5030.
[17] R. Mustafa Öksüzoglu, T.E. Weirich, H. Fuess, J. Electron Microsc. 52 (2) (2003) 91.
[18] S.-H. Ge, Z.Z. Zhang, Y.-Y. Lu, C.-X. Li, R.-J. Gan, Thin Solid Films 311 (1997) 33.
[19] Y.D. Zhang, J.I. Budnick, W.A. Hines, C.L. Chien, J.Q. Xiao, J. Appl. Phys. 72 (1998) 2053.